Supporting Information for

Optimizing oxygen reduction catalytic activity of bipyridine-based polymer through tuning molecular weight

Binbin Wang, Weichen Song, Daohao Li, Xiaojing Long,* Yanzhi Xia

*To whom correspondence should be addressed. E-mail: Xiaojing Long (longxj@qdu.edu.cn)

Contents:

1. Structural and morphology characterization

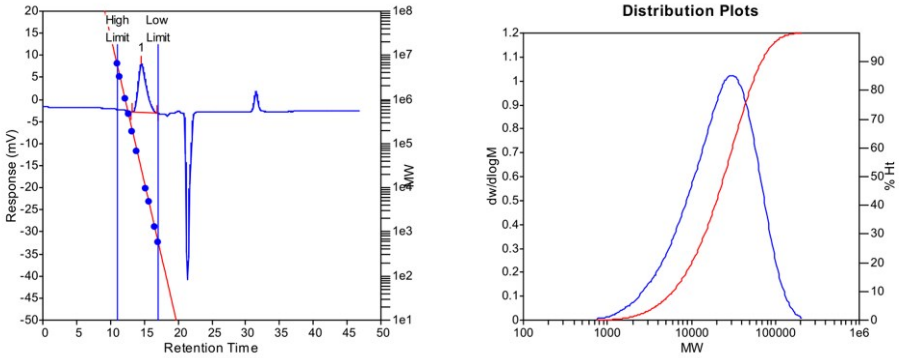

Fig. S1 GPC traces of **PBIPYT$_L$**.

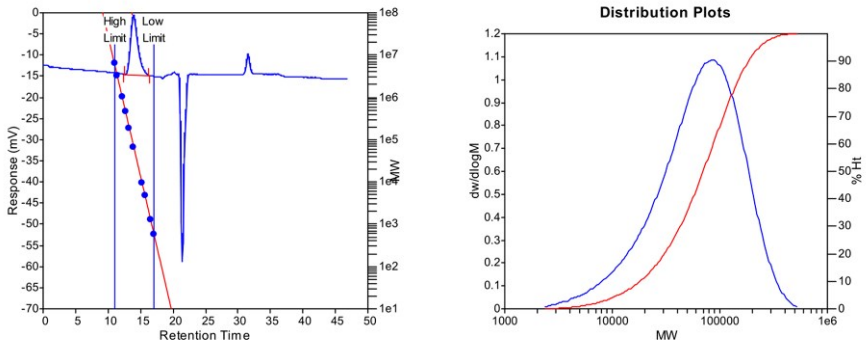

Fig. S2 GPC traces of **PBIPYT$_M$**.

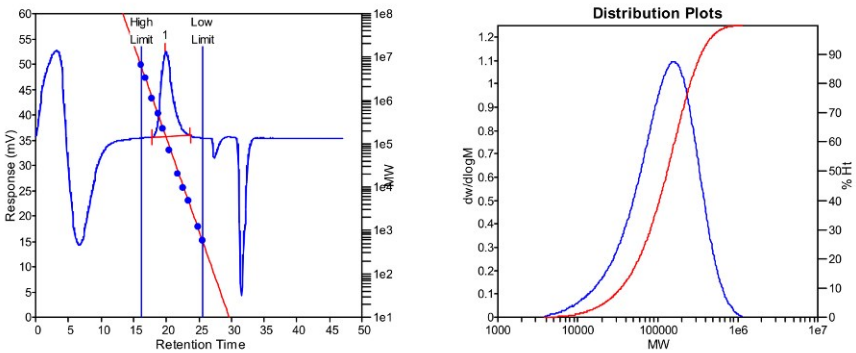

Fig. S3 GPC traces of **PBIPYT$_H$**.

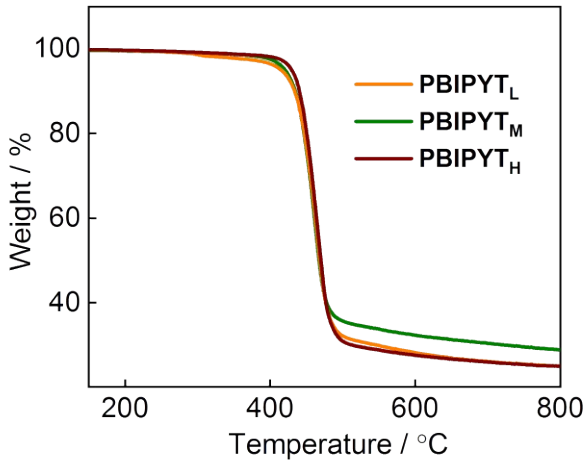

Fig. S4 TGA curves of **PBIPYT$_L$**, **PBIPYT$_M$** and **PBIPYT$_H$**.

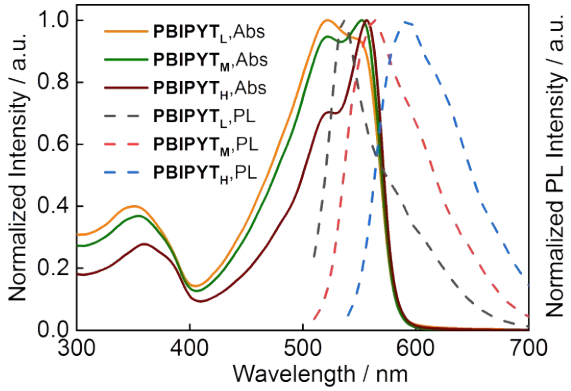

Fig. S5 UV-vis absorption and fluorescence spectra of **PBIPYT$_L$**, **PBIPYT$_M$** and **PBIPYT$_H$** in CH_2Cl_2.

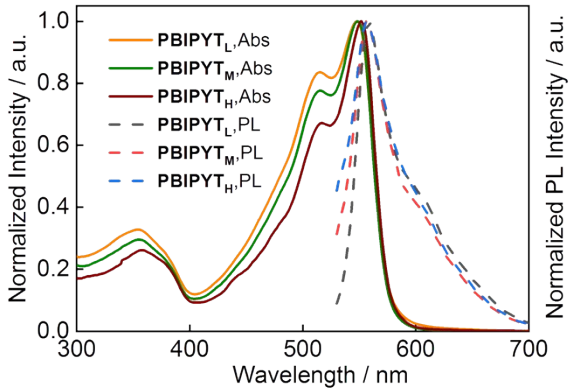

Fig. S6 UV-vis absorption and fluorescence spectra of **PBIPYT$_L$**, **PBIPYT$_M$** and **PBIPYT$_H$** in hexane.

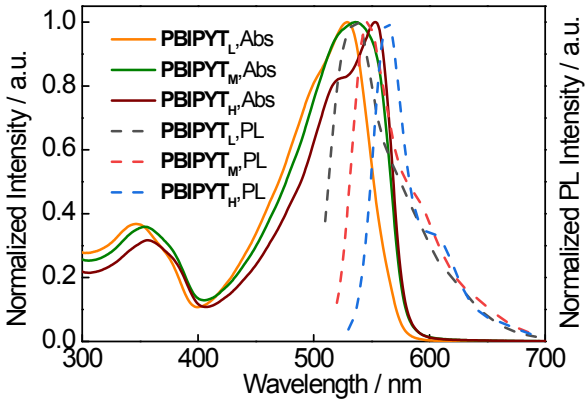

Fig. S7 UV-vis absorption and fluorescence spectra of **PBIPYT$_L$**, **PBIPYT$_M$** and **PBIPYT$_H$** in THF.

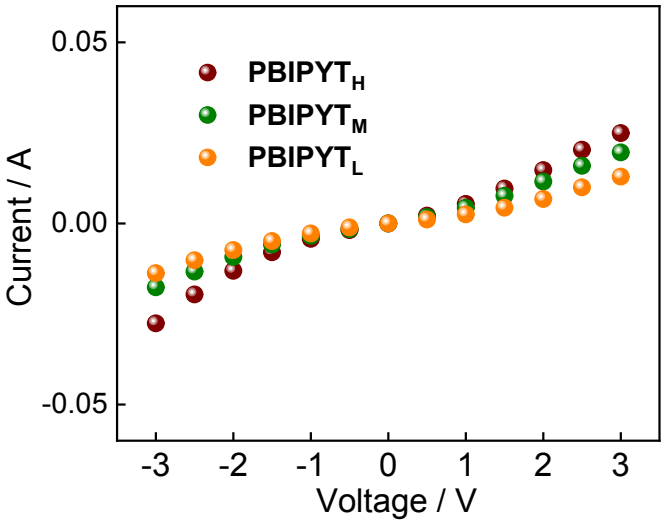

Fig. S8 Room temperature current (I)-voltage (V) curves of **PBIPYT$_H$**, **PBIPYT$_M$** and **PBIPYT$_L$**.

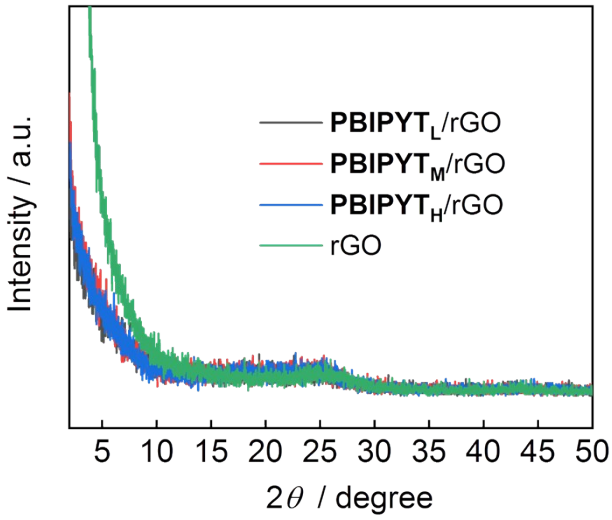

Fig. S9 X-ray diffraction patterns of **PBIPYT$_L$**/rGO**, PBIPYT$_M$**/rGO, **PBIPYT$_H$**/rGO and rGO.

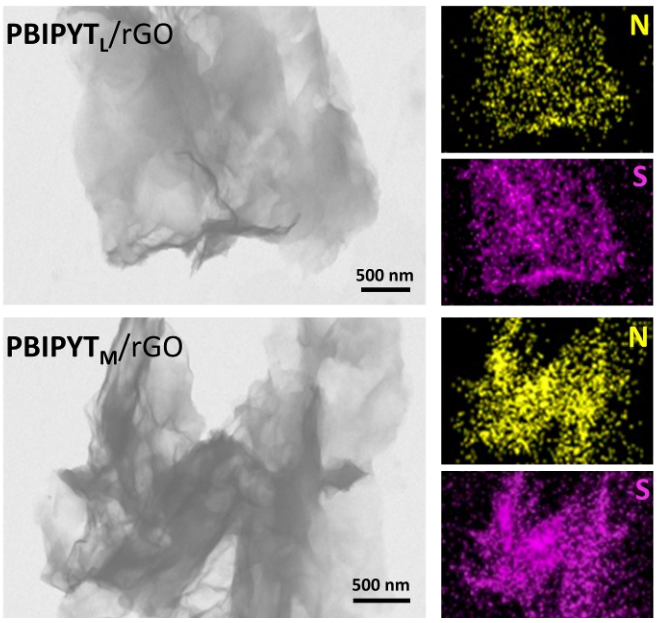

Fig. S10 TEM images of **PBIPYT$_L$**/rGO and **PBIPYT$_M$**/rGO and the corresponding EDS mapping for S and N elements.

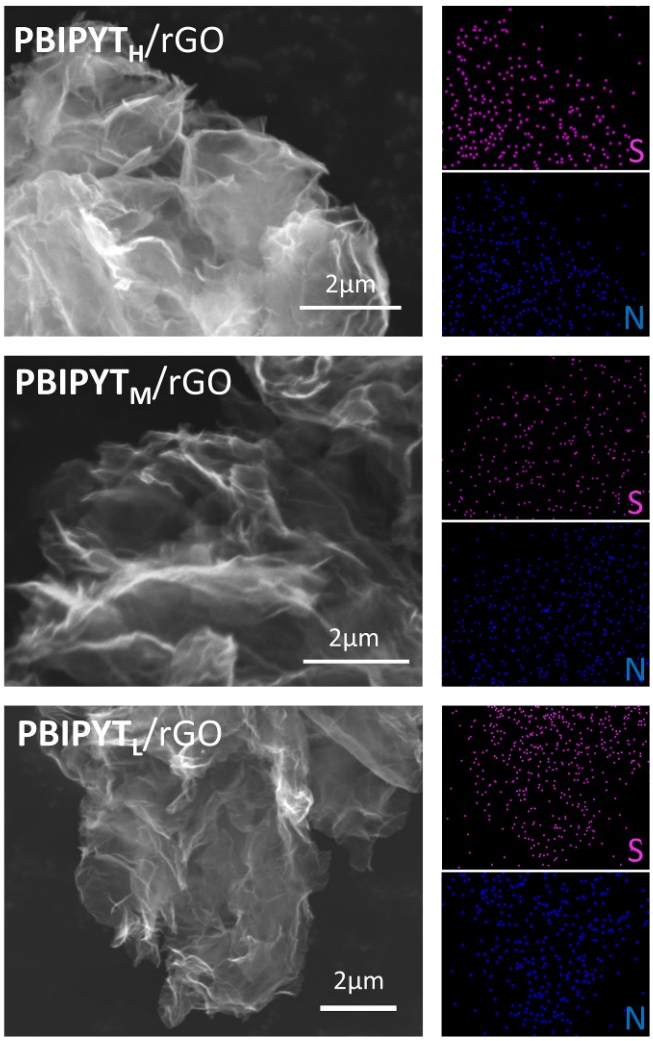

Fig S11 SEM image of **PBIPYT$_H$**/rGO, **PBIPYT$_M$**/rGO and **PBIPYT$_L$**/rGO and the corresponding EDS mapping for S and N elements.

2. Electrochemical ORR performance

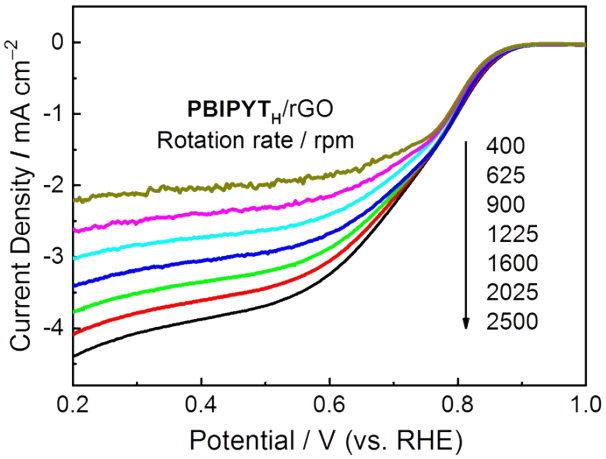

Fig. S12 LSV curves of **PBIPYT$_H$**/rGO at various rotation speeds.

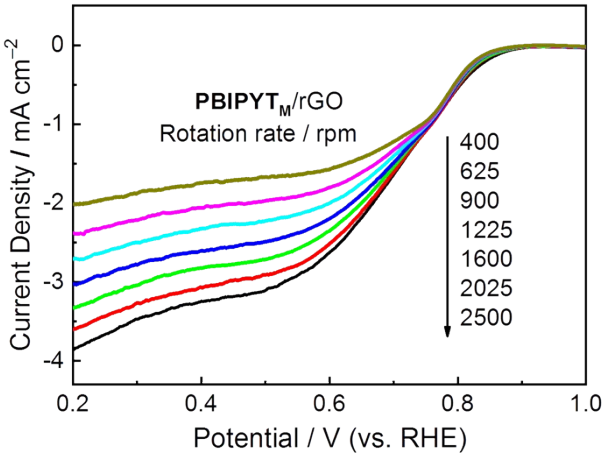

Fig. S13 LSV curves of **PBIPYT$_M$**/rGO at various rotation speeds.

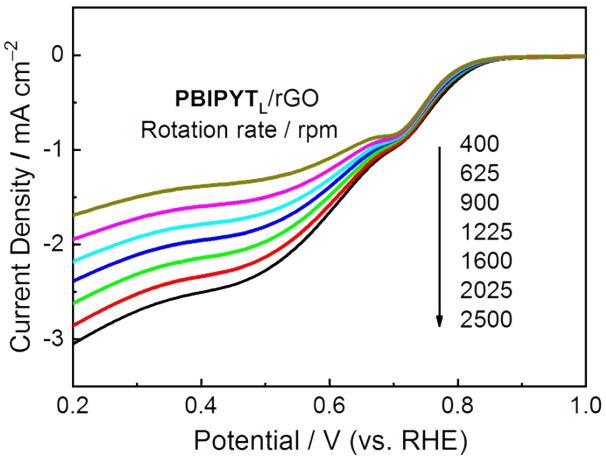

Fig. S14 LSV curves of **PBIPYT$_L$**/rGO at various rotation speeds.

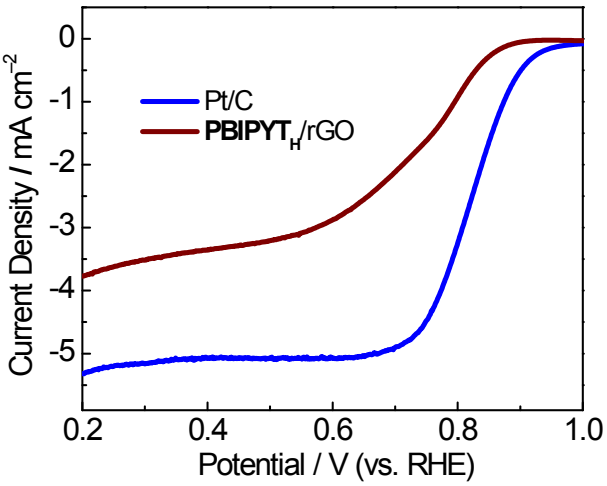

Fig. S15 LSV curves of **PBIPYT$_H$**/rGO and Pt/C in O_2-saturated in 0.1 M aq KOH at 1600 rpm.

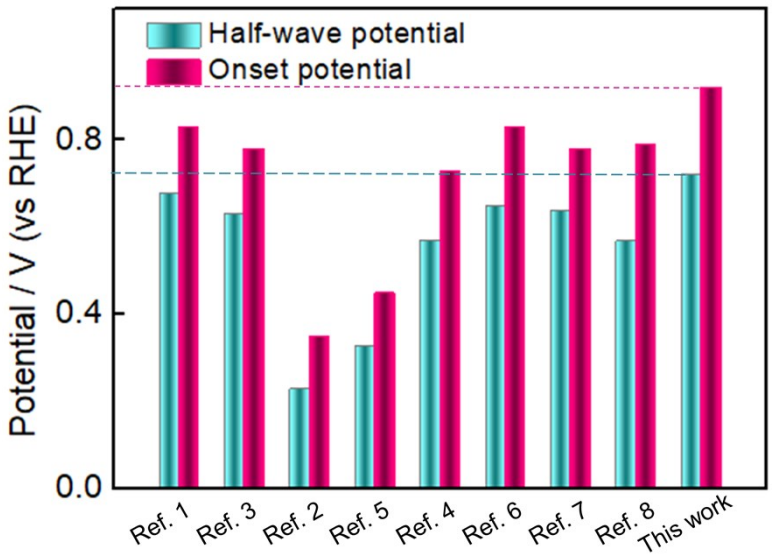

Fig. S16 The onset and half-wave potential distributions of reported metal-free polymer-based catalysts and **PBIPYT$_H$**/rGO (this work).[1-8]

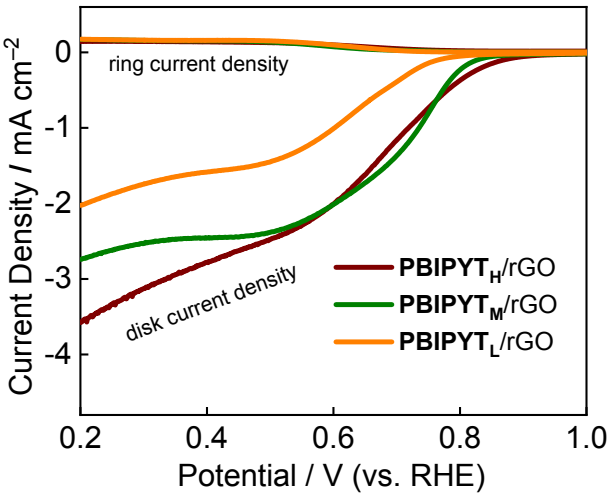

Fig. S17 The RRDE polarization curve of **PBIPYT$_H$**/rGO, **PBIPYT$_M$**/rGO and **PBIPYT$_L$**/rGO.

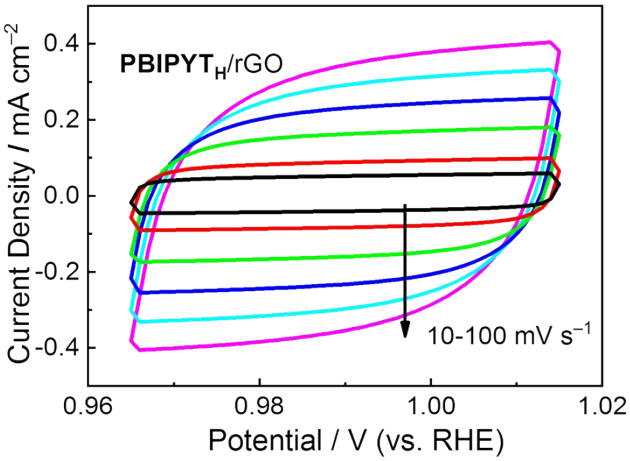

Fig. S18 CVs of **PBIPYT$_H$**/rGO in 0.1 M KOH solution at different scan rates (10, 20, 40, 60, 80, and 100 mV s^{-1}).

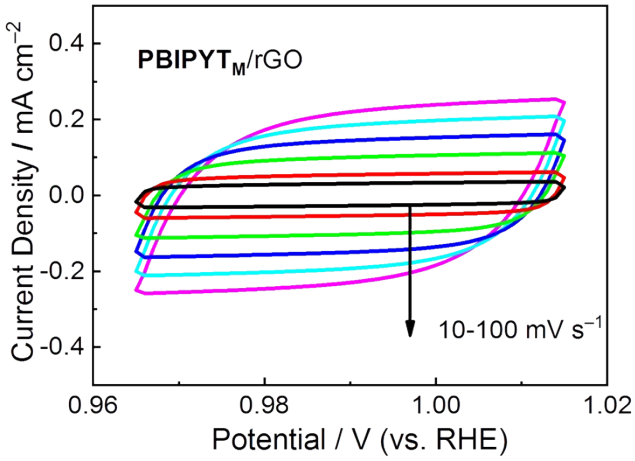

Fig. S19 CVs of **PBIPYT$_M$**/rGO in 0.1 M KOH solution at different scan rates (10, 20, 40, 60, 80, and 100 mV s^{-1}).

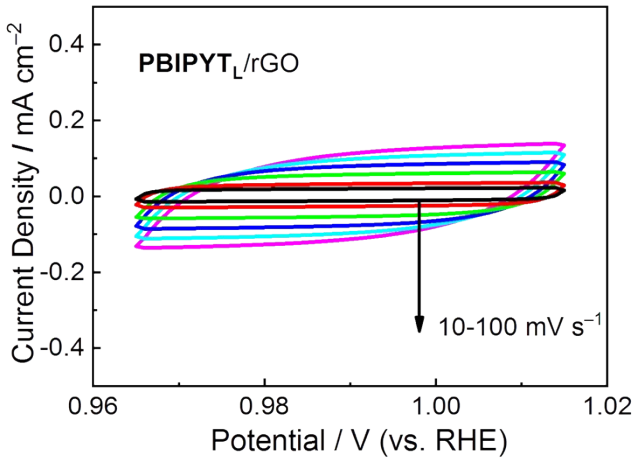

Fig. S20 CVs of **PBIPYT$_L$**/rGO in 0.1 M KOH solution at different scan rates (10, 20, 40, 60, 80, and 100 mV s^{-1}).

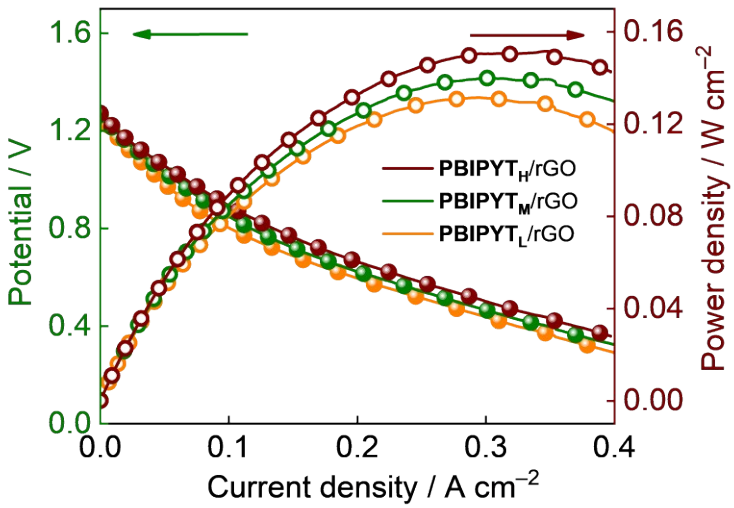

Fig. S21 Discharge polarization curve and corresponding power density plot of **PBIPYT$_H$**/rGO, **PBIPYT$_M$**/rGO and **PBIPYT$_L$**/rGO

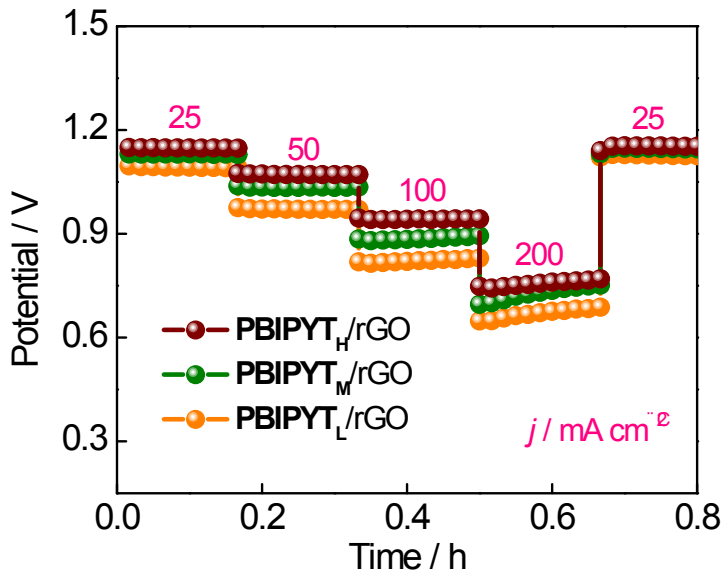

Fig. S22 Discharge curves of **PBIPYT$_H$**/rGO-, **PBIPYT$_M$**/rGO- and **PBIPYT$_L$**/rGO-based ZABs at different current densities (25, 50, 100, 200 mA cm^{-2}).

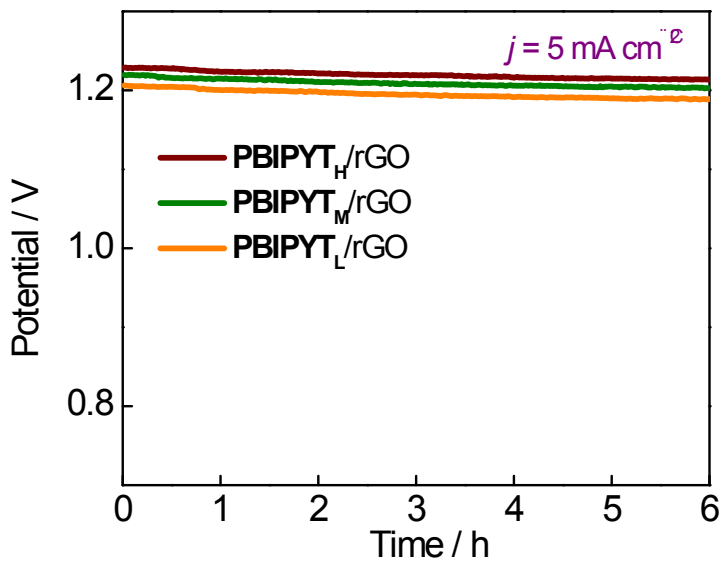

Fig. S23 Galvanostatic discharge curve of **PBIPYT$_H$**/rGO-, **PBIPYT$_M$**/rGO- and **PBIPYT$_L$**/rGO-based ZABs (6.0 M KOH electrolyte).

3. DFT calculations

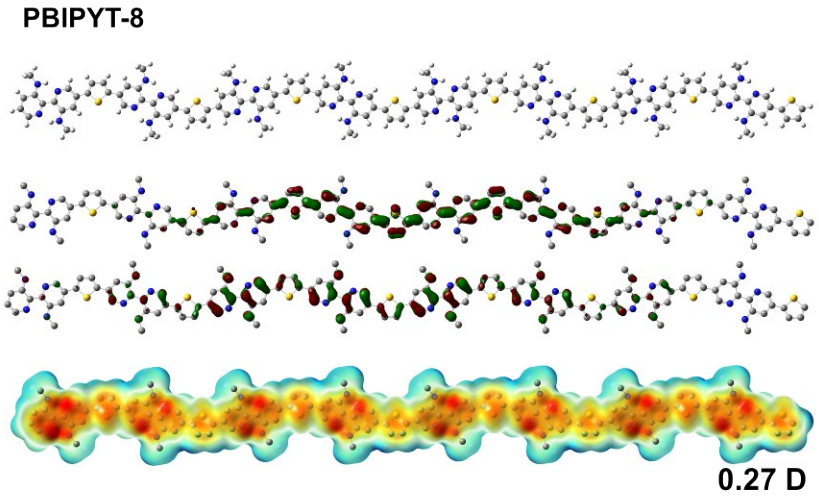

Fig. S24 The optimized model structure of PBIPYT-8. Kohn–Sham molecular orbitals of the model compound of PBIPYT-8 (B3LYP/6-31G*).[9] The electrostatic potential surface maps and dipole moment for PBIPYT-8.

4. NMR spectra

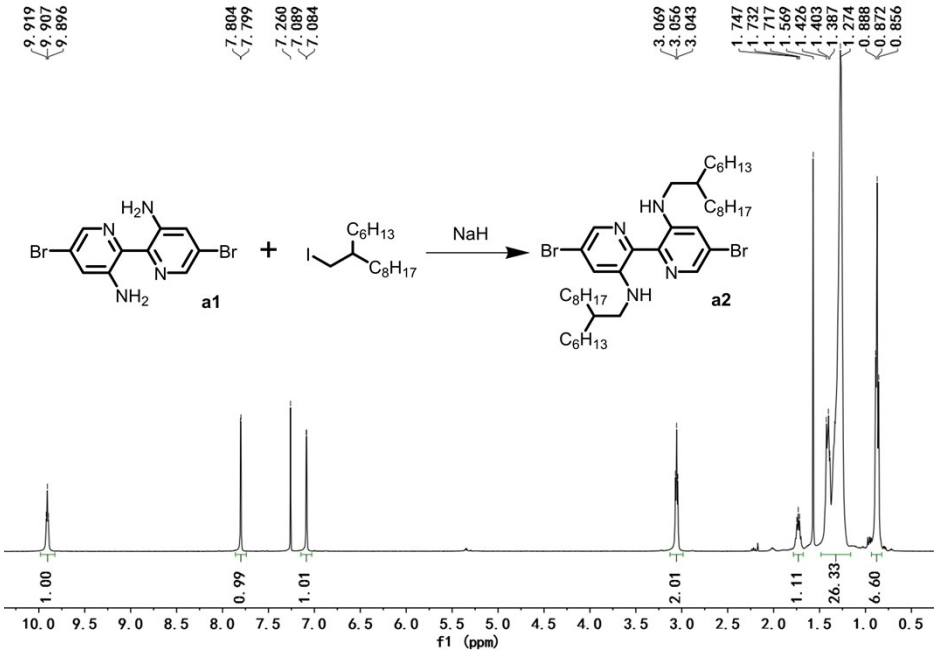

Fig. S25 ^{1}H NMR spectrum of **a2**.

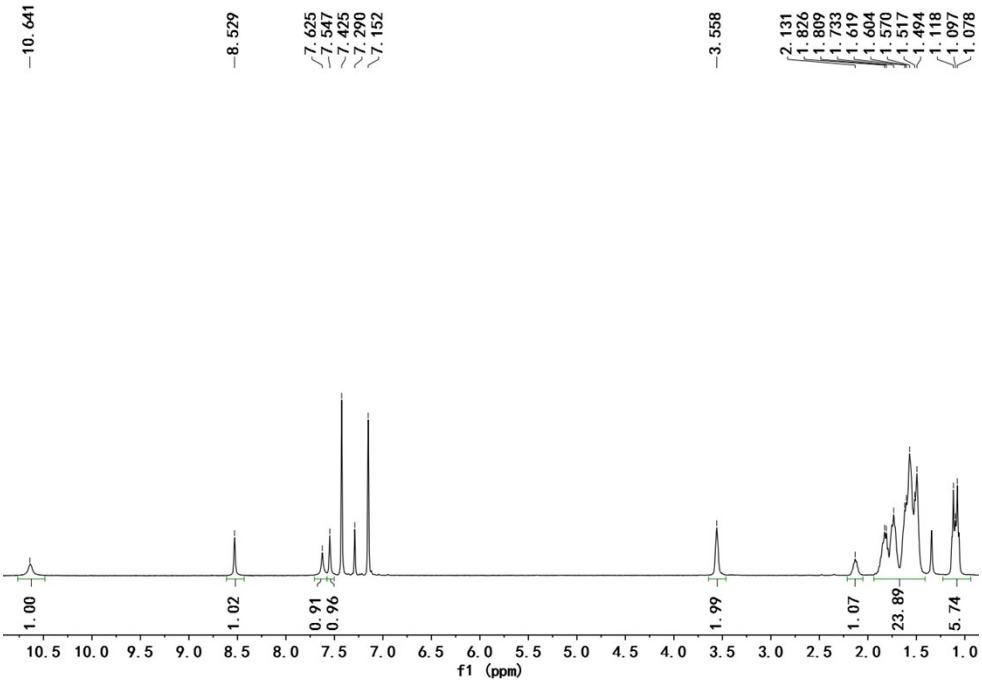

Fig. S26 ^{1}H NMR spectrum of **PBIPYT$_L$**.

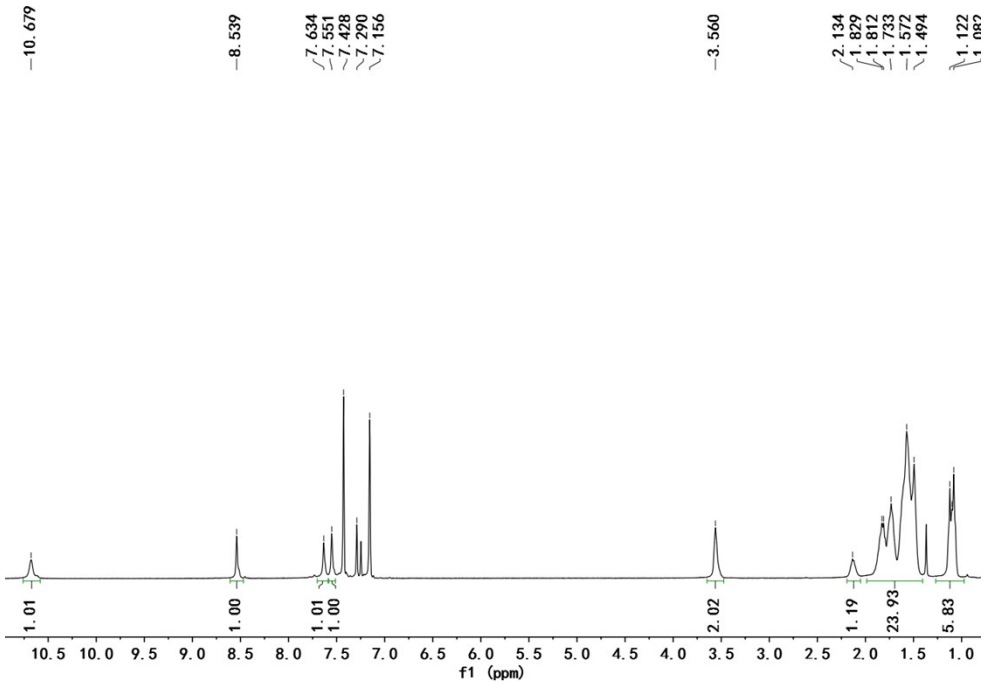

Fig. S27 ^{1}H NMR spectrum of **PBIPYT$_{M}$**.

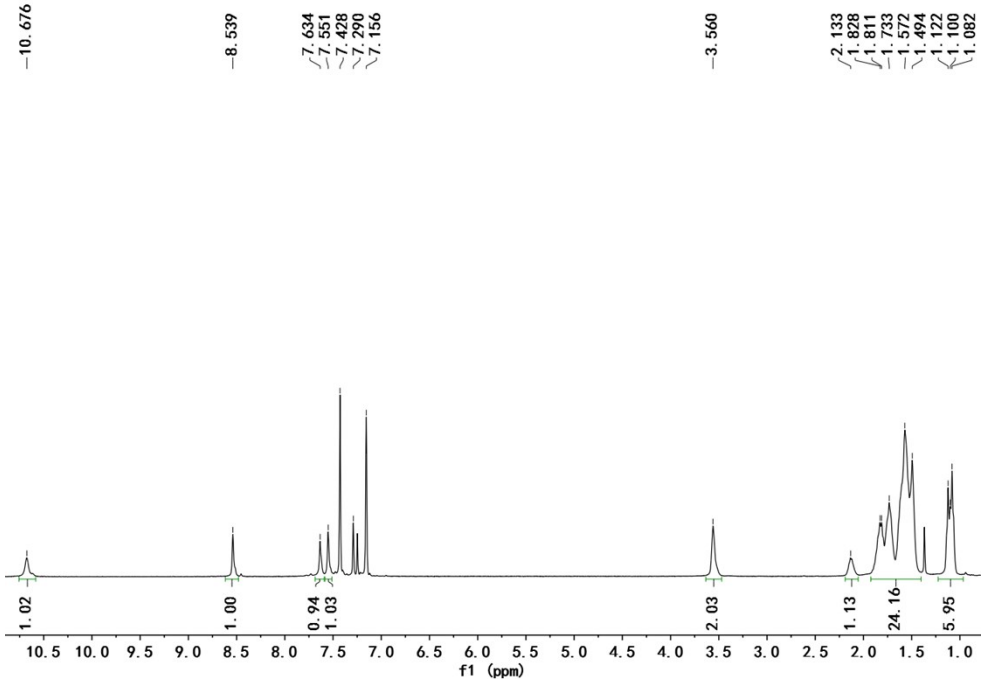

Fig. S28 ^{1}H NMR spectrum of **PBIPYT$_{H}$**.

5. References

[1] J. Guo, C.-Y. Lin, Z. Xia, Z. Xiang, *Angew. Chem. Int. Ed.* **2018**, *130*, 12747–12752.

[2] H. He, M. Wang, Y. Zhang, J. Zhao, *J Solid State Electrochem*. **2017**, *21*,1639–1651.

[3] S. Roy, A. Bandyopadhyay, M. Das, P. P. Ray, S. K. Pati, T. K. Maji, *J. Mater. Chem. A* **2018**, *6*, 5587–5591.

[4] B. Devi, R. R. Konerb, A. Halder, *New J.Chem.* **2017**, *41*, 7972−7979.

[5] Y. Chu, L. Gu, X. Ju, H. Du, J. Zhao, K. Qu, *Catalysts* **2018**, *8*, 245–264.

[6] S. G. Patnaik, R. Vedarajan, N. Matsumi, *ACS Appl. Energy Mater.* **2018**, *1*, 1183–1190.

[7] S. Bhattacharyya, D. Samanta, S. Roy, V. P. Haveri Radhakantha, T. K. Maji, *ACS Appl. Mater. Interfaces* **2019**, *11*, 5455−5461.

[8] T.-N. Pham-Truong, H. Randriamahazaka, J. Ghilane, *ACS Catal.* **2018**, *8*, 869−875.

[9] Gaussian 09 (Revision A.02), M. J. Frisch, G. W. Trucks, H. B. Schlegel, G. E. Scuseria, M. A. Robb, J. R. Cheeseman, G. Scalmani, V. Barone, B. Mennucci, G. A. Petersson, H. Nakatsuji, M. Caricato, X. Li, H. P. Hratchian, A. F. Izmaylov, J. Bloino, G. Zheng, J. L. Sonnenberg, M. Hada, M. Ehara, K. Toyota, R. Fukuda, J. Hasegawa, M. Ishida, T. Nakajima, Y. Honda, O. Kitao, H. Nakai, T. Vreven, J. A. Montgomery, Jr., J. E. Peralta, F. Ogliaro, M. Bearpark, J. J. Heyd, E. Brothers, K. N. Kudin, V. N. Staroverov, R. Kobayashi, J. Normand, K. Raghavachari, A. Rendell, J. C. Burant, S. S. Iyengar, J. Tomasi, M. Cossi, N. Rega, J. M. Millam, M. Klene, J. E. Knox, J. B. Cross, V. Bakken, C. Adamo, J. Jaramillo, R. Gomperts, R. E. Stratmann, O. Yazyev, A. J. Austin, R. Cammi, C. Pomelli, J. W. Ochterski, R. L. Martin, K. Morokuma, V. G. Zakrzewski, G. A. Voth, P. Salvador, J. J. Dannenberg, S. Dapprich, A. D. Daniels, Ö. Farkas, J. B. Foresman, J. V. Ortiz, J. Cioslowski, D. J. Fox, *Gaussian, Inc*., Wallingford CT, **2009**.